

Ξ^- atomic X-ray spectroscopy using a counter-emulsion hybrid method

M. Fujita^{1,*}, H. Ekawa², Y. Endo³, R. Goto³, S. Hasegawa¹, S. H. Hayakawa⁴, K. Hayashi³, R. Honda⁵, K. Hoshino³, K. Hosomi¹, M. Ichikawa^{1,6}, Y. Ichikawa¹, H. Ito³, Y. Ishikawa⁴, W. S. Jung⁷, A. Kasagi^{2,8}, S. H. Kim¹, S. Kinbara⁸, H. Kobayashi³, T. Koike⁴, J. Y. Lee⁹, P. M. Lin⁸, Y. Nagase³, D. Nakashima³, K. Nakazawa^{3,8}, T. Nanamura^{1,6}, N. Nishimura³, S. Nishimura³, A. N. L. Nyaw⁸, M. Ohashi³, H. Sako¹, M. K. Soe³, H. Tamura^{1,4}, A. M. M. Theint³, K. T. Tint³, Y. Toyama¹⁰, M. Ukai^{4,5}, T. O. Yamamoto¹, S. B. Yang⁷, J. Yoshida⁴, M. Yoshimoto¹¹, and D. Zhang¹²

¹Advanced Science Research Center, Japan Atomic Energy Agency, Tokai 319-1195, Japan

²High Energy Nuclear Physics Laboratory, RIKEN, Wako 351-0198, Japan

³Faculty of Education, Gifu University, Gifu 501-1193, Japan

⁴Department of Physics, Tohoku University, Sendai 980-8578, Japan

⁵Institute of Particle and Nuclear Studies, High Energy Accelerator Research Organization (KEK), Tsukuba 305-0801, Japan

⁶Department of Physics, Kyoto University, Kyoto 606-8502, Japan

⁷Department of Physics, Korea University, Seoul 02841, Korea

⁸Graduate School of Engineering, Gifu University, Gifu 501-1193, Japan

⁹Seoul National University, Seoul 08826, South Korea

¹⁰Center for Muon Science and Technology, Chubu University, Kasugai 487-8501, Japan

¹¹RIKEN Nishina Center, RIKEN, 2-1 Hirosawa, Wako, Saitama 351-0198, Japan

¹²Institute of Modern Physics, Shanxi Normal University, Taiyuan 030031, China

*E-mail: fujitam@post.j-parc.jp

Received June 25, 2022; Revised November 13, 2022; Accepted November 23, 2022; Published November 25, 2022

.....
 Ξ^- atomic X-ray spectroscopy is one of the most useful methods for investigation of the Ξ^- -nucleus strong interaction. Since the X-ray energy is shifted and/or broadened due to the Ξ^- -nucleus strong interaction compared to those calculated from electromagnetic interaction alone, the measurement of the energy shift, ΔE , and the width, Γ , give us information on the Ξ^- -nucleus potential. A serious problem in the measurement is the significant background derived from in-flight Ξ^- decay. A novel method of identifying stopped Ξ^- events using the nuclear emulsion was developed to realize the first Ξ^- atomic X-ray spectroscopy experiment as the J-PARC E07 experiment, which also aimed at searching for $\Lambda\Lambda$ and Ξ^- hypernuclei in the emulsion. The X-rays emitted from Ξ^- Br and Ξ^- Ag atoms were measured using germanium detectors. No clear peaks were observed in the obtained spectra. However, we succeeded in reducing the background to 1/170 by this method employing coincidence measurements using nuclear emulsion and X-ray detectors.

Subject Index D01

1. Introduction

Elucidation of the interaction between a nucleon (N) and a hyperon (Y) is the first step toward understanding the strong interaction between baryons under the SU(3) flavor symmetry. The NN interaction has been investigated by employing rich and extensive data obtained from NN

scattering experiments. On the other hand, conducting scattering experiments with hyperons such as Λ , Σ , and Ξ , is challenging due to their short lifetimes of the order of 100 ps. The YN and YY interactions have been investigated utilizing the properties of nuclei with hyperons (hypernuclei) and exotic atoms with negatively charged hyperons (hyperatoms).

Experimental studies on the systems with S (strangeness) = -1 , such as Λ and Σ hypernuclei, have progressed as reviewed in Refs. [1,2]. These studies, alongside theoretical investigations, provided insights into the ΛN and ΣN interactions. The ΛN interaction, which is attractive with a potential depth of 30 MeV for Λ hyperons in nuclear matter, has been studied using binding energy data of various light-to-heavy Λ hypernuclei, and detailed studies on the spin dependence of the ΛN interaction have also been made. The ΣN interaction was found to be attractive at the nuclear surface using Σ atomic X-ray spectroscopy [3,4], but it was also found to be repulsive inside the nucleus [5]. Recently, a Σp scattering experiment has been successfully conducted at the Japan Proton Accelerator Research Complex (J-PARC) [6,7]. It is expected that future scattering experiments using Λ and Σ hyperon beams will provide direct information on the ΛN and ΣN interactions.

However, for $S = -2$ systems, experimental data are severely limited. The Ξ -nucleus interactions have been experimentally studied in Ξ^- hypernuclei and Ξ^- atoms using two methods. One is missing mass spectroscopy, in which Ξ^- hypernuclei are directly produced by replacing a proton in the target nucleus with a Ξ^- hyperon via the (K^-, K^+) reaction, and the other uses nuclear emulsion to observe Ξ^- atoms and Ξ^- hypernuclei formed after the Ξ^- atomic capture and absorption by a nucleus. Missing mass spectroscopy of the (K^-, K^+) reaction for $S = -2$ hypernuclei using magnetic spectrometers was conducted in the KEK-PS E224 [8] and the BNL E885 [9] experiments. In these experiments, no clear Ξ^- hypernuclear peaks were observed due to low statistics and limited resolution, and they only suggested that the depth of the real part of the Ξ -nucleus potential is about 10–20 MeV. On the other hand, an experimental method searching for $S = -2$ systems using nuclear emulsion was developed in the KEK-PS E176 [10] and E373 [11] experiments. The KISO event observed in the E373 experiment, in which a Ξ^- - ^{14}N bound system decayed to twin Λ hypernuclei, revealed that the Ξ -nucleus interaction is attractive [12]. At J-PARC, upgraded experiments of these two types (E05/E70 [13] and E07 [14]) were proposed. In 2016–2017, the emulsion experiment (E07) aiming at producing ten times more $S = -2$ events than the KEK E373 experiment was conducted, and observations of several $S = -2$ hypernuclear events were reported. In the MINO event, a Ξ^- hyperon was absorbed by an oxygen nucleus and produced a $\Lambda\Lambda$ hypernucleus. Adopting the most probable interpretation of the event as $^{11}_{\Lambda\Lambda}\text{Be}$, the binding energy of two Λ hyperons, $B_{\Lambda\Lambda}$, was obtained as 19.07 ± 0.11 MeV [15]. In the IBUKI and IRRAWADDY events, Ξ^- hyperons were absorbed by nitrogen nuclei and produced twin hypernuclei. The IBUKI event was interpreted as $\Xi^- + ^{14}\text{N} \rightarrow ^{10}_{\Lambda}\text{Be} + ^5_{\Lambda}\text{He}$, and the binding energy of a Ξ^- hyperon, B_{Ξ} , was obtained as 1.27 ± 0.21 MeV [16]. The IRRAWADDY event was interpreted as $\Xi^- + ^{14}\text{N} \rightarrow ^5_{\Lambda}\text{He} + ^5_{\Lambda}\text{He} + ^4\text{He} + n$, and B_{Ξ} was uniquely obtained as 6.27 ± 0.27 MeV [17].

In this paper, we report on another experimental approach, Ξ^- atomic X-ray spectroscopy, which can provide valuable information about the Ξ -nucleus interaction complementary to the B_{Ξ} values described above. Just as the hadron-nucleus interactions have been studied with exotic atoms, such as pionic, kaonic, and Σ^- atoms, the Ξ -nucleus interaction can be studied with Ξ^- atoms. The energy levels of a Ξ^- atom are shifted, and their widths are broadened due to the Ξ -nucleus strong interaction compared to those calculated with the Coulomb in-

teraction alone. The shifts and the widths can be obtained by measuring the X-rays associated with deexcitation. If the width of the hypernuclear state is very large or the state cannot be uniquely assigned for each of the observed events, the real and imaginary parts of the nuclear potential cannot be determined well from the binding energy data (or the mass spectrum) of the hypernucleus. In the case of X-ray spectroscopy, the numerical values of the shifts and the widths of the X-rays are unambiguously connected to the real and imaginary parts of the strong interaction optical potential. Since the X-ray spectroscopy is sensitive to the surface region of the Ξ -nucleus potential, combining the X-ray and the hypernuclear mass data allows us to investigate the shape of the Ξ -nucleus potential. The first experiment of Ξ^- atomic X-ray spectroscopy was conducted as the J-PARC E07 experiment using nuclear emulsion alongside the experiment searching for $\Lambda\Lambda$ and Ξ^- ($S = -2$) hypernuclei.

2. X-ray spectroscopy of Ξ^- atoms

2.1 Experimental principle

Since the Ξ^- hyperon has a negative charge, it forms a Ξ^- atom via the Coulomb interaction with the nucleus. A Ξ^- atomic state is characterized by the principal quantum number, n , and the angular momentum quantum number, l . Firstly, the Ξ^- hyperon is captured in a state with a large n (~ 50) and l . In many cases, it cascades down to the inner orbits via some Auger transitions, and then radiative transitions. Since the circular orbits (the largest l orbit ($l = n - 1$) among the same n states) have the largest population probability during exotic atom formation, the cascade process of E1 transitions further concentrates the population in the circular orbits. Finally, the Ξ^- hyperon is absorbed by the nucleus via the strong interaction, $\Xi^- p \rightarrow \Lambda\Lambda$. At the nuclear surface, the probability that the Ξ^- hyperon is absorbed by the nucleus is comparable to the probability that the Ξ^- hyperon cascades down to the next inner orbit via an E1 transition. In the further inner orbits, absorption by the nucleus dominates and no transition X-rays are observed. The E1 transition just before the dominant absorption is called the “last” transition. The next higher transition to the last transition is referred to as the “upper” transition in this paper.

When the Ξ -nucleus potential is represented by U , the strong interaction optical potential, U_{str} , can be extracted by subtracting the known Coulomb interaction potential, U_{Coul} , from U , and written as $U_{\text{str}}(r) = V(r) + iW(r)$. The energy shift (ΔE) of the atomic state is given by the following formula:

$$\Delta E = \langle \Phi^{n,l} | H_{\text{kin}}(r) + U_{\text{Coul}}(r) + V(r) | \Phi^{n,l} \rangle - \langle \Phi^{n,l} | H_{\text{kin}}(r) + U_{\text{Coul}}(r) | \Phi^{n,l} \rangle, \quad (1)$$

where $|\Phi^{n,l}\rangle$ and $|\Phi'^{n,l}\rangle$ are the (n, l) eigenstates with and without the strong interaction, and $H_{\text{kin}}(r)$ is the kinematical part of the Hamiltonian. If the Ξ -nuclear interaction is attractive (repulsive) at the nuclear surface, the shift value is positive (negative). The width for the Ξ^- potential absorption from the (n, l) state, $\Gamma_{\text{abs}}^{(n,l)}$, is given as follows [18]:

$$-\frac{i}{2}\Gamma_{\text{abs}}^{(n,l)} = \langle \Phi^{n,l} | iW(r) | \Phi^{n,l} \rangle. \quad (2)$$

Measuring ΔE and Γ_{abs} provides information about the potentials $V(r)$ and $W(r)$, respectively. Outside the nucleus, where the Ξ -nucleus strong interaction is weak, ΔE and Γ_{abs} are too small to measure. On the other hand, the last transition occurs at the nuclear surface and contains the most significant information on the strong interaction potential via sizable ΔE and Γ_{abs} values. Only the E1 transition between the circular orbits, $(n + 1, l + 1) \rightarrow (n, l)$ with $l = n -$

1, is usually considered as the last transition. In the case of the Ξ^- Ag atom discussed in this paper, the last transition is ($8J \rightarrow 7I$) and its energy is 370 keV. In such an energy region, the Auger process is negligible. The energy shift in the upper orbit is negligibly small compared to that in the last orbit; thus the measured X-ray shift can be regarded as a shift in the last orbit.

The branching ratio of the last transition of $(n + 1, l + 1) \rightarrow (n, l)$ with $l = n - 1$, BR_{last} , is given as a function of Γ_{abs} and the known E1 transition rates, Γ_{E1} , as follows:

$$BR_{\text{last}} = \frac{\Gamma_{\text{E1}}((n + 1, n) \rightarrow (n, n - 1))}{\Gamma_{\text{E1}}((n + 1, n) \rightarrow (n, n - 1)) + \Gamma_{\text{abs}}(n + 1, n)}. \quad (3)$$

BR_{last} is also approximately equal to the ratio of the last transition yield to the upper transition $(n + 2, n + 1) \rightarrow (n + 1, n)$ yield, because the $(n + 1, n)$ state is expected to be populated almost entirely via the $(n + 2, n + 1) \rightarrow (n + 1, n)$ transition. When BR_{last} is experimentally determined from the yields of two X-rays, $\Gamma_{\text{abs}}(n + 1, n)$ is obtained from Eq. (3) with the calculated $\Gamma_{\text{E1}}((n + 1, n) \rightarrow (n, n - 1))$ value, and information about the imaginary potential $W(r)$ can be extracted. Assuming that the nuclear absorption rate is negligibly small before the last transition, the yield of the upper E1 transition can be estimated by a cascade calculation considering exclusively the Coulomb interaction. Thus, the potential $W(r)$ can also be discussed in terms of the yield of the last transition only.

2.2 Experimental difficulty

The Ξ^- atomic X-ray measurements entail a substantial experimental difficulty. Because of the large recoil momentum of a Ξ^- hyperon produced in the $p(K^-, K^+)\Xi^-$ reaction and its short lifetime of 164 ps, most of the Ξ^- hyperons decay before stopping and produce significant background. The main decay mode is $\Xi^- \rightarrow \Lambda\pi^-$ (branching ratio 99.9%). When a Λ decays as $\Lambda \rightarrow p\pi^-$, the resultant π^- is absorbed by the surrounding material and produces background γ rays and neutrons. On the other hand, when a Λ decays as $\Lambda \rightarrow n\pi^0$ followed by $\pi^0 \rightarrow 2\gamma$, they also produce the background. Tagging Ξ^- stop events is key to overcoming this difficulty.

We developed a new method adopting coincidence measurement using nuclear emulsion and X-ray detectors. The detection of Ξ^- hyperons using emulsion images enabled the identification of Ξ^- stop events with high reliability and a clean X-ray spectrum with a good signal-to-noise ratio (S/N) was obtained. Taking advantage of the $S = -2$ hypernuclear search experiment using emulsion, simultaneous X-ray measurements were proposed. The experiment was conducted as the J-PARC E07 experiment. The Ξ^- atoms of C, N, O, Br, and Ag, which are contained in the emulsion, can be produced. The experiment was optimized for Ξ^- Br and Ξ^- Ag atomic X-ray measurements, because more than half of the stopped Ξ^- hyperons, $(56.8 \pm 4.6)\%$, were captured by Br or Ag atoms [19].

2.3 Theoretical prediction

In the case of Br and Ag atoms, the last transitions of Ξ^- hyperons were expected to be the Br($7I \rightarrow 6H$) and Ag($8J \rightarrow 7I$) transitions, respectively. Their energies were calculated as 370 keV and 316 keV, respectively, without considering the strong interaction. Assuming two theoretical models, i.e., the $t\rho$ potential and the density-dependent (DD) potential constructed from the Nijmegen D (ND) interaction [20], the shift and the width values were predicted as shown in Table 1 (E. Friedman and A. Gal, private communications). Both potentials have been corrected to reproduce the depth of $V_0 = 14$ MeV. The $t\rho$ potential is a phenomenological optical potential proportional to the hadron–nucleon scattering amplitude and a nuclear density dis-

Table 1. Theoretical prediction of the last transition energy, E_X , for Ξ^- Br and Ξ^- Ag atoms (E. Friedman and A. Gal, private communications).

Transition	Potential	E_X w/o strong int. [keV]	Shift [keV]	Width [keV]
Br($7I \rightarrow 6H$)	$t\rho$	315.5	0.73	0.44
	ND		5.5	1.74
Ag($8J \rightarrow 7I$)	$t\rho$	370.4	0.28	0.15
	ND		3.3	0.79

tribution, $\rho(r)$. The DD potential is constructed from the density-dependent Ξ - n interaction in matter derived via the G-matrix method (YNG interaction [21]) based on the Nijmegen D interaction model [22]. Among several versions of the Nijmegen model, the ΞN interaction is attractive in model D. Incidentally, the energies of the upper transitions, Br($8J \rightarrow 7I$) and Ag($9K \rightarrow 8J$), were estimated as 206 keV and 255 keV, respectively, considering the Coulomb potential with a point charge. In the case of C, N, and O atoms, the last transitions of Ξ^- hyperons are expected to be the $4F \rightarrow 3D$ transitions with energies of 55 keV, 76 keV, and 101 keV, respectively.

The absolute yield of the X-ray transition was estimated from a cascade calculation, which considered the loss of the Ξ^- hyperon during the cascading process as well as all the transitions and Auger processes. The probability that the captured Ξ^- hyperon cascades down and reaches the (n, l) state is denoted as $P_{\Xi}(nl)$. Batty et al. estimated the P_{Ξ} value using the calculation code developed for muonic atoms and later modified it to take into account the strong interaction so as to reproduce Σ^- Pb atom data [20]. The P_{Ξ} value of the upper orbit for Ξ^- Pb atom is calculated to be 0.6. For kaonic atoms, the value of this probability for the upper state has a small variation between species [23]. Assuming a similar situation in the case of Ξ^- atoms, the $P_{\Xi}(8J)$ value is assumed to be 0.6. The absolute yield of the last transition $(n+1, n) \rightarrow (n, n-1)$ is evaluated as $Y_{\Xi \text{ atom}} \cdot P_{\Xi}(n+1) \cdot BR(E1(n+1, n) \rightarrow (n, n-1))$, where $Y_{\Xi \text{ atom}}$ is the number of the produced Ξ^- atoms.

3. Experiment

In the present experiment, Ξ^- hyperons were produced via the (K^-, K^+) reaction using a K^- beam supplied at J-PARC. The primary protons were accelerated every 5.5 s and extracted to the Hadron Experimental Facility during a beam extraction period (spill) of 2.2 s. A total of 4.3×10^{13} protons per spill were accelerated to 30 GeV (corresponding to the accelerator power of 37 kW) and irradiated onto a primary gold target. Then, the produced secondary beam was transported to the experimental target through the K1.8 beam line.

In the experiment, coincidence measurement of stopped Ξ^- hyperons and X-rays was realized. A schematic drawing of the experimental setup is shown in Fig. 1. The setup comprised three parts: two magnetic spectrometers for identifying the Ξ^- production reaction, tracking detectors for Ξ^- hyperons, and a germanium (Ge) detector array for X-ray measurement. A cross-sectional view of the target surroundings is shown in Fig. 2. The Ξ^- hyperons produced by the (K^-, K^+) reaction on a diamond target (9.87 g/cm² thick) were injected into and stopped in the emulsion installed downstream of the target, and the events of Ξ^- atoms and hypernuclei were identified by emulsion image analysis after the beam irradiation. The Ge detectors were

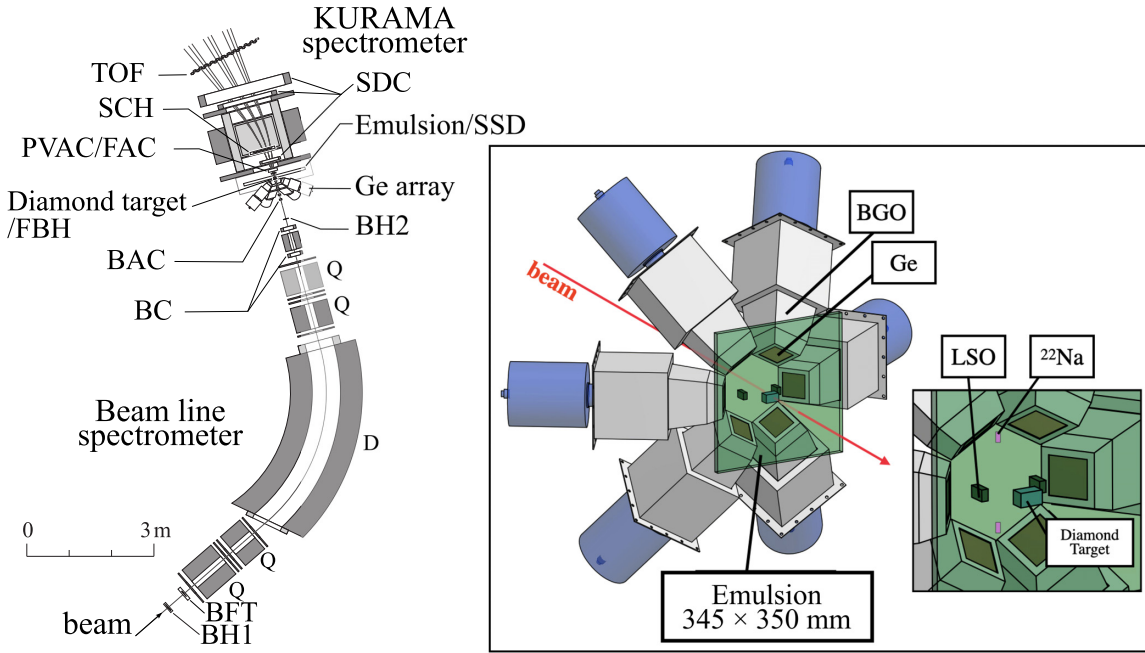


Fig. 1. Experimental setup. The beam line spectrometer and the KURAMA spectrometer consist of hodoscopes (BH1, BH2, FBH, SCH, and TOF), a beam fiber tracker (BFT), aerogel Cherenkov counters (BAC, PVAC, and FAC), drift chambers (BC and SDC), and silicon strip detectors (SSD). The inset shows the emulsion detector and a germanium detector array.

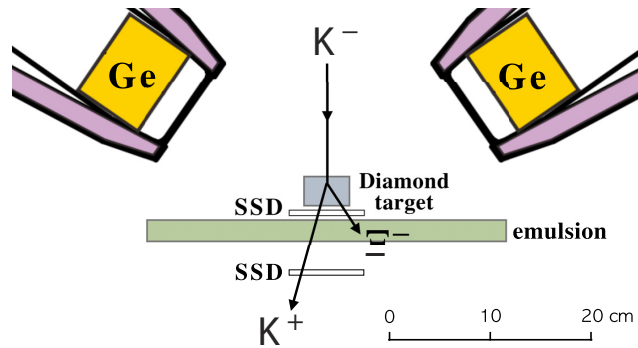


Fig. 2. Cross-sectional view of around the target.

installed around the emulsion, and Ξ^- atomic X-rays emitted from the emulsion were detected. The point where a Ξ^- hyperon reached the emulsion surface was predicted using the magnetic spectrometers and the Ξ^- hyperon tracking detectors. Thanks to the adopted counter-emulsion hybrid method, it was possible to restrict the emulsion area that required scanning by optical microscopes to an order of 0.1 mm^2 per track, and the time of image analysis was drastically shortened.

3.1 Beam line and target

The K1.8 beam line at J-PARC is suitable for Ξ^- hyperon production since it is designed to supply K^- beams with momenta up to $1.8 \text{ GeV}/c$, which maximizes the $p(K^-, K^+)\Xi^-$ reaction cross section [24]. The K1.8 beam line has two sets of electrostatic separators and mass slits for discarding pion and other secondary particle contamination. In this experiment, a $1.8 \text{ GeV}/c$

secondary K^- beam of $2.8 \times 10^5/\text{spill}$ with a π^- contamination of $6.0 \times 10^4/\text{spill}$ was transported to the experimental target at the K1.8 area. In total, 11.4×10^{10} K^- mesons were used to produce Ξ^- hyperons via the (K^-, K^+) reaction.

Diamond was used as the Ξ^- production target, which also served as an energy degrader for the produced Ξ^- hyperons. The size of the target was $5.06^W \times 3.03^H \times 3.04^T$ cm³, and its thickness was 9.87 g/cm².

3.2 Missing mass spectroscopy system

Two magnetic spectrometers were employed for the missing mass spectroscopy of the (K^-, K^+) reaction. The incident K^- and scattered K^+ particles were analyzed by the K1.8 beam line spectrometer and the KURAMA spectrometer, respectively. The K1.8 beam line spectrometer consisted of a $QQDQQ$ magnet system with two plastic counter hodoscopes (BH1 and BH2), a tracking detector made of scintillating fibers (BFT), and two drift chambers (BCs) for measuring the time of flight and trajectory. It also had aerogel Cherenkov counters with a refractive index $n = 1.03$ (BACs) to reject contaminant π^- particles present in the beam. The momentum bite of the transported secondary beam was $\pm 3\%$ and the momentum resolution ($\delta p/p$) was 3.3×10^{-4} (FWHM) [25]. The KURAMA spectrometer with a large solid angle of 280 msr and a moderate momentum resolution ($\delta p/p$) of 2.8×10^{-2} was employed, because the large acceptance was more important than the resolution for the present experiment using the counter-emulsion hybrid method. The KURAMA spectrometer comprises a dipole magnet, plastic counter hodoscopes (FBH, SCH, and TOF), drift chambers (SDCs), and aerogel Cherenkov counters (PVAC and FAC). The PVAC with an index $n = 1.12$ was used to reject scattered protons with momenta lower than 1.6 GeV/ c , and the FAC with an index $n = 1.05$ was used to reject pions with momenta higher than 0.45 GeV/ c and unscattered beam kaons. The trigger for the data acquisition of the (K^-, K^+) reaction events (“ KK trigger”) was generated by combining the responses of the aerogel Cherenkov counters and the hodoscopes. The trigger rate was 0.6 kHz.

3.3 Ξ^- tracking detectors

Ξ^- hyperon tracks were measured by two sets of silicon strip detectors (SSD). One SSD was placed between the target and the emulsion, and the other SSD was just downstream of the emulsion (see Fig. 2). The sensitive area of the SSDs was $76.8^W \times 76.8^H$ mm² with a strip pitch of 50 μm , and each detector had four layers. The upstream SSD measured the track and energy deposit of the Ξ^- hyperons emitted from the target to predict the position on the emulsion surface that the Ξ^- hyperons reached. The pulse height of the upstream SSD was also used to select Ξ^- hyperons with velocities slow enough to be stopped within the emulsion. The downstream SSD was used to reject those events in which Ξ^- hyperons passed through the emulsion and for analysis of the scattered K^+ tracks.

The size of the emulsion was $345^W \times 350^H$ mm² and a single emulsion module consisted of 13 emulsion sheets. Thin emulsion sheets, consisting of two 0.1-mm thick emulsion layers on a 0.18-mm thick polystyrene base, were placed at both faces of the emulsion module to measure the angle of penetration tracks. Thick emulsion sheets with two 0.48-mm thick emulsion layers were adopted for the remaining 11 sheets. The typical density of the employed emulsion was 3.53 g/cm³. The emulsion modules were installed in an emulsion mover and automatically moved during the beam irradiation. The position on the emulsion surface exposed to the beam

particles was changed with every spill so that the whole area of the emulsion sheets could be exposed almost uniformly. A total of 118 modules were exposed to the beam.

3.4 X-ray spectroscopy system

To measure the last transitions of Ξ^- Br and Ξ^- Ag atoms, Ge detectors were employed due to their good energy resolution of 0.8 keV in σ at 400 keV. A Ge detector array, consisting of six detectors and a calibration system [26], was constructed and placed around the emulsion module. A trigger for X-ray detection was generated when the Ge array registered a hit at the same time as the *KK* trigger, and the energy and timing information was recorded. The effective energy range of our Ge array was from 100 to 1400 keV. The time resolution of each Ge detector was 14–21 ns in FWHM at 200–300 keV. The Ge array was located near the reaction target, where high-energy particles and photons were produced by a high-energy (1.8 GeV/ c) and high-rate (1.6×10^5 particles/s) beam. In these conditions, the gain of the Ge detectors was slightly changed due to a large energy deposit rate to the detectors, which must not be ignored in the measurement of the small X-ray energy shifts. For background suppression, each Ge detector was surrounded by $\text{Bi}_4\text{Ge}_3\text{O}_{12}$ (BGO) scintillation counters. When γ rays were Compton-scattered in the Ge detector or high-energy charged particles from the beam penetrated the Ge detector, some of them were detected in the BGO counters and rejected as the background (BGO suppression). To correct the in-beam gain change, a novel calibration system consisting of Lu_2SiO_5 (LSO) scintillation counters and ^{22}Na sources was developed, making it possible to constantly acquire in-beam calibration data simultaneously with the Ξ^- atomic X-ray data. The X-ray energy was calibrated using three reference γ rays, the 307-keV and 202-keV γ rays from ^{176}Lu naturally present in the LSO scintillator as well as the 511-keV γ ray from the ^{22}Na source. Consequently, a calibration with an uncertainty of less than ± 100 eV was achieved. Details of the performance of the Ge detector array and the new energy calibration method are available in Ref. [26].

4. Analysis

4.1 Analysis of magnetic spectrometers

For emulsion image analysis, the (K^- , K^+) reaction events reconstructed via particle identification and tracking using the magnetic spectrometers were selected. The particles were identified by the mass calculated from the time of flight together with the momentum and the flight path length obtained by track reconstruction analysis.

The incident K^- mesons were identified by analyzing the beam line spectrometer data. The trajectories and the momenta of the beam particles were not significantly dispersed. K^- and π^- particles in the beam were discriminated sufficiently well using the time of flight between the two hodoscopes, BH1 and BH2. It was found that there was almost no π^- contamination in the data recorded by the *KK* trigger. Note that even though π^- was rejected by the trigger, it could pass through the emulsion and contribute to the background for image analysis.

The scattered K^+ mesons were identified by analyzing the KURAMA spectrometer data. The trajectories were obtained by chi-squared fitting of the hit positions at the tracking detectors located upstream and downstream of the KURAMA magnet. The momenta of scattered particles were obtained by analyzing the motion in the magnetic field of the KURAMA magnet using the Runge–Kutta method [28]. The K^+ mesons were selected in the obtained mass distribution of the scattered particles.

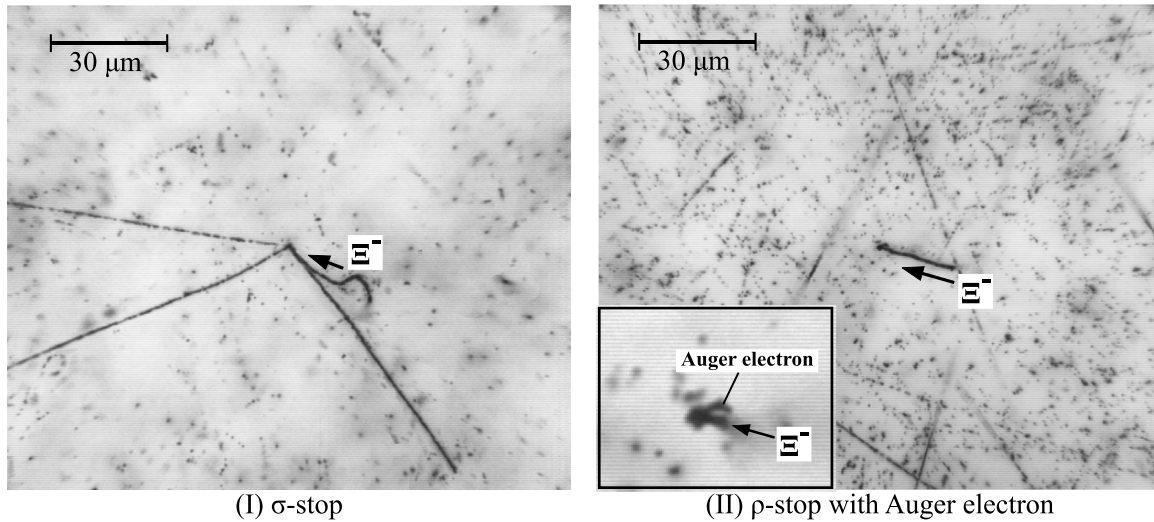


Fig. 3. Photographs of stopped Ξ^- hyperons (indicated by arrows) observed in the emulsion. (I) σ -stop: one or more charged fragments/particles were observed at the Ξ^- stopping point. (II) ρ -stop: no charged tracks was observed. An Auger electron was sometimes emitted as shown in the enlarged view (bottom left).

The reconstructed K^- and K^+ tracks were combined to analyze the (K^-, K^+) reaction, and the events with the reconstructed vertex point in the target region were selected. The produced Ξ^- tracks were precisely determined using the hit information from the upstream SSD. Consistency between the x and y positions of K^- mesons at the target and the vertex point reconstructed from the K^+ and Ξ^- tracks was checked. Also, consistency between the direction of the reconstructed missing momenta and the measured Ξ^- tracks was checked. For rejection of the Ξ^- hyperons that passed through the emulsion module, it was also required that there were no hits by the Ξ^- hyperon in the downstream SSD.

As described above, the incident K^- and scattered K^+ were selected, and events were selected in which the vertices of those tracks were within the reaction target. Furthermore, the consistency with the Ξ^- track detected by SSD was also confirmed. Details of the analysis procedure and cutoff thresholds are provided in Refs. [29,30]. As a result, the selected Ξ^- events correspond to 80% of the expected yield in simulation.

4.2 Analysis of emulsion images

For the events selected by the reaction analysis, the emulsion images were analyzed. Detection of Ξ^- tracks in the emulsion images was conducted using a microscope and an automated tracking system [30]. Using a Ξ^- track reconstructed by the SSD, an area of $0.4 \text{ mm} \times 0.4 \text{ mm}$ around the predicted point on the emulsion was scanned. A total of 1207 emulsion sheets, comprising 93% of their total number, were scanned. As of September 2021, 35 438 candidate tracks have been scanned automatically and subsequently classified manually.

A Ξ^- hyperon stopped in the emulsion was observed as one of the following two types of images. In the first type, charged fragments were produced after the Ξ^- hyperon stopped. In Fig. 3(I), one or more charged fragments/particles can be observed at the Ξ^- hyperon stopping point. Such events were classified as “ σ -stop” events. In the second type, as shown in Fig. 3(II), no charged particle tracks were observed at the stopping point. This happened when only neutral particles, including n , Λ , and π^0 , were produced in the Ξ^- absorption process, or when

Table 2. Number of stopped events identified from emulsion analysis.

	Without Ge coincidence	With Ge coincidence
σ -stop	2208	779
σ -stop without short prong	–	488
ρ -stop	9961	2660
ρ -stop with Auger e^-	–	75

heavy fragments were produced but their tracks were too short to be observed. Such events were classified as “ ρ -stop” events. In the case of Ξ^- ρ -stop, Auger electrons emitted during cascading were sometimes observed, as shown in the enlarged image in Fig. 3(II). Even though only the Ξ^- hyperons stopped in the emulsion were aimed at, other events such as Ξ^- in-flight decay or Ξ^- passing through the emulsion were also found, and they had to be removed manually. The numbers of stop events identified from the emulsion analysis are listed in Table 2: there were 2208 and 9961 σ - and ρ -stop events, respectively.

Almost all the σ -stop events, except for a small percentage of π^- contamination, are Ξ^- events. Considering that the ratio of σ -stops to ρ -stops reported in Ref. [10] is 2:1, the number of Ξ^- ρ -stop events was expected to be around 1100. The other events classified as the ρ -stop events were caused by particles other than Ξ^- hyperons, such as protons. By selecting events accompanied by an Auger electron, contamination can be removed and the S/N ratio improved. However, this criterion would not provide complete identification because it is known that in ρ -stop events only $(40.4 \pm 6.8)\%$ of stopped Ξ^- hyperons emit an Auger electron [10]. Among the 2660 ρ -stop events with coincidence hits registered by the Ge array, an Auger electron was observed in 75 of them.

For the σ -stop events, identification of Ξ^- absorption on “heavy” nuclei (Br and Ag) was adopted. Emissions of low-energy charged particles from heavy nuclei are inhibited by the Coulomb barrier. Events with a short prong of 3–31 μm are interpreted as the events of Ξ^- absorption on “light” nuclei (C, N, and O) [10]. The presence of a short prong was checked for the 779 σ -stop events with coincidence hits in the Ge detectors. By selecting events without a short prong, 488 events were identified.

Misclassification of a non- σ -stop event as a σ -stop event may occur during visual analysis by the human eye. The ratio of events that were misclassified as σ -stop was evaluated by five independent analysts using a subset of the data, and it was obtained as $(13.8 \pm 2.9)\%$. In addition, σ -stop events included 3% of π^- contamination. Considering jointly the misclassifications and contamination, the percentage of Ξ^- absorption events included among the identified σ -stop event set was evaluated to be $(83.6 \pm 2.8)\%$.

4.3 Analysis of X-rays

To remove the accidental background, only the data for which the Ge hit timing coincided with the KK trigger timing were analyzed. Since the time resolution of the Ge detectors depended on the photon energy, the timing gate was set as a function of the energy. The energy information was calibrated for each Ge detector every hour using the in-beam calibration method, and then the energy spectra obtained by all the Ge detectors were summed up. The efficiency of the Ge detectors, ϵ_{Ge} , contains the full-energy peak efficiency, the live time of the readout electronics, and the data-acquisition efficiency. The full-energy peak efficiency of the Ge detectors,

Table 3. Relative systematic uncertainties for stopped events.

Source	Uncertainty [%]
Emulsion analysis	3.4
ϵ_{Ge}	11.4
ϵ_{BGO}	1.5
Percentage of Ξ^- captured to heavy atoms (E373)	6.7
Total	13.7

which considers the acceptance of the crystals and the photoabsorption effects of the diamond target and the emulsion, was calibrated using a standard source in the off-beam conditions. It was determined to be $(0.84 \pm 0.09)\%$ at 370 keV for the data-acquisition period after May 2017 corresponding to the irradiation of 90 emulsion modules. The live time of the readout system was calibrated using a standard source in the on-beam conditions and was determined to be $(88 \pm 1.0)\%$. Furthermore, considering the data-acquisition efficiency of 95%, the total efficiency of the Ge detectors, ϵ_{Ge} , was obtained as $(0.7 \pm 0.08)\%$. The timing information of the BGO counters was recorded, and the events in which the BGO counters surrounding the Ge detector with a hit registered a signal simultaneously with the trigger were removed. The Ge detector signal may be accidentally killed by this BGO suppression. The survival ratio of the Ge signal through the BGO suppression, ϵ_{BGO} , was evaluated to be $(83.9 \pm 1.3)\%$ using the 718-keV γ ray peak from the ^{10}B excited state, which was observed in the in-beam γ -ray spectrum. The total efficiency, considering both ϵ_{Ge} and ϵ_{BGO} , was $(0.59 \pm 0.07)\%$ at 370 keV. The details of the X-ray analysis are explained in Ref. [26].

4.4 Systematic uncertainty

Systematic uncertainties for the X-ray yield are summarized in Table 3. Since this uncertainty is for selected stopped events, the uncertainties in the analysis of the magnetic spectrometers were not included. The total systematic uncertainty is obtained to be 13.7% by summing all individual uncertainties in quadrature.

5. Results and discussion

The X-ray energy spectra focusing on the energy region of the last and upper transitions for Ξ^- Br and Ξ^- Ag atoms were obtained and are shown in Fig. 4. Data from all scanned emulsion modules were used to produce these spectra, and the BGO suppression was applied to all of them. The top spectrum (a) is for the Ξ^- production events identified by the reaction analysis, the middle one (b) is a summed spectrum for the σ -stop events and the “ ρ -stop with Auger electron” events, and the bottom one (c) is for the “ σ -stop without short prong” events and the “ ρ -stop with Auger electron” events.

The X-ray peaks were searched for in the (b) and (c) spectra. Using the maximum likelihood method, the X-ray spectra were fitted by a Gaussian plus a background function, assuming a constant offset as the background spectrum. The amplitude of the Gaussian function (amp) and the constant offset were the fitting parameters, while the mean and sigma of the Gaussian function were fixed to a certain value (E_{mean}) and the resolution of 0.8 keV, respectively. The E_{mean} value was scanned in steps of 1 keV within the search region. The peak significance N_σ was defined as $N_\sigma = amp/amp_{\text{error}}$, where amp_{error} was the fitting error for the amp value. For

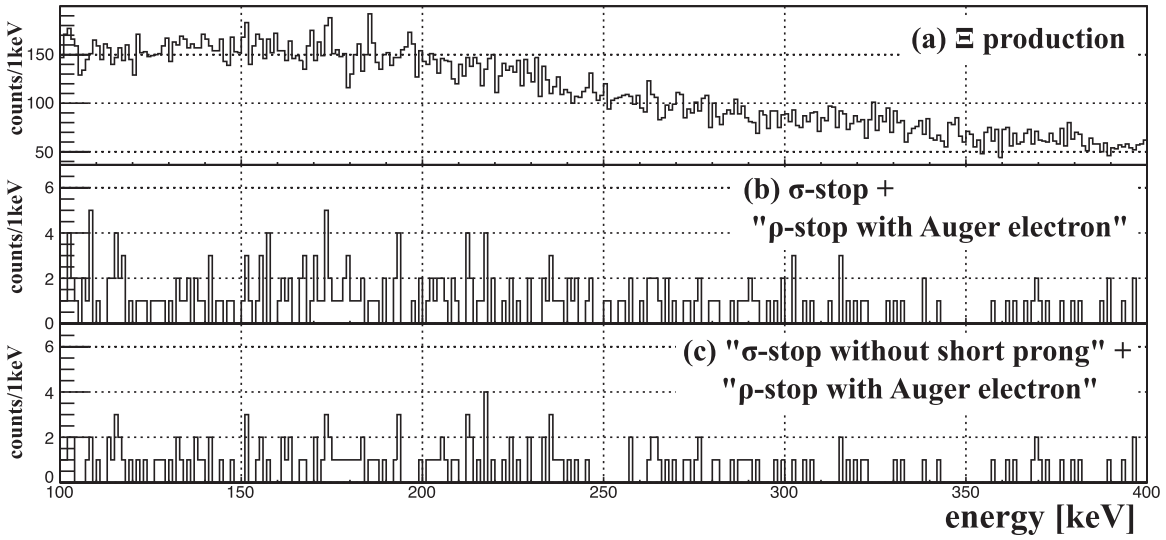


Fig. 4. X-ray spectra (a) for the Ξ^- production by (K^- , K^+) reaction analysis (top), (b) for the σ -stop events and the “ ρ -stop with Auger electron” events selected by emulsion image analysis (middle), and (c) for the “ σ -stop without short prong” events and the “ ρ -stop with Auger electron” (bottom).

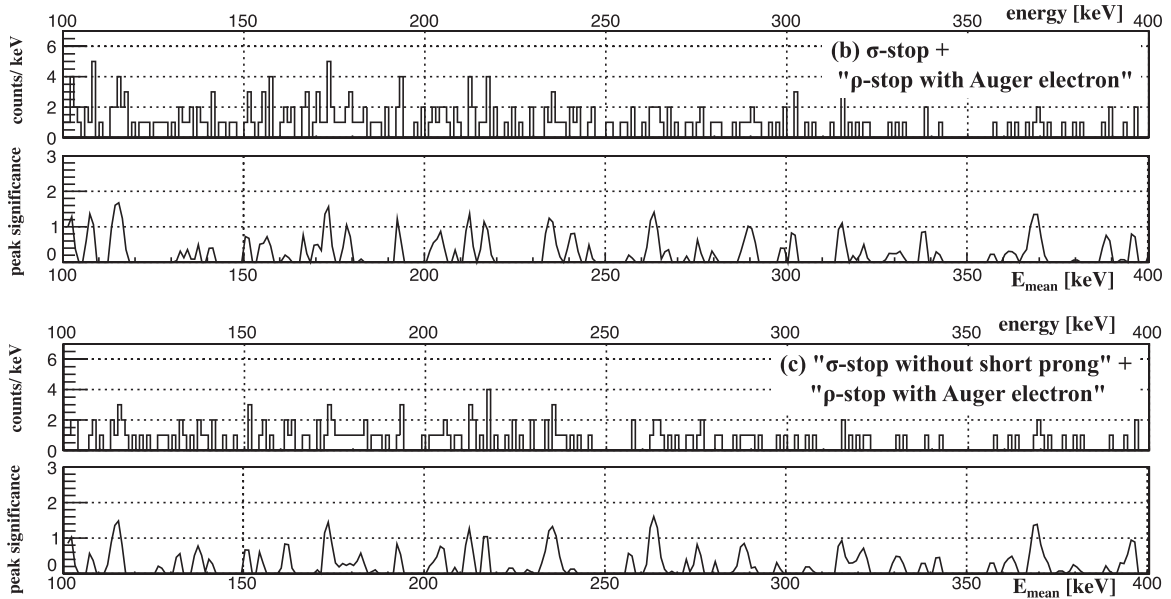


Fig. 5. Peak significance for spectra (b) from Fig. 4 for the σ -stop events and the “ ρ -stop with Auger electron” events, and (c) for the “ σ -stop without short prong” events and the “ ρ -stop with Auger electron” events.

the spectra (b) and (c), the peak significance obtained as a function of E_{mean} is shown in Fig. 5. From this analysis, no evident peak with a significance larger than 3σ was found. The spectra were fitted with various sigma values, 0.8, 2, 3, 4, and 5 keV, but no evident peak was observed in any case. Further searches were carried out in other energy regions, but no peak was found either (see Appendix A). From this peak search, the upper limit of the X-ray yield, $Y_{\text{X-ray}}$, was obtained as a function of E_{mean} .

Assuming that the X-ray yield was small enough, the background level was evaluated as shown in Table 4 for each selection. The spectrum (a) for Ξ^- production selection was fitted

Table 4. Background level of X-ray spectra (data for all emulsion modules).

Conditions		Background level [counts/keV]
(a)	Ξ^- production	63.5
(b)	σ -stop+ ρ -stop with Auger e^-	0.37
	σ -stop	0.34
(c)	σ -stop without a short prong+ ρ -stop with Auger e^-	0.28
	σ -stop without a short prong	0.25

with a linear function, and its background level was obtained as 63.5 counts/keV at 370 keV. The spectra (b) and (c) were fitted with only a constant function. The background level was evaluated as $0.37^{+0.86}_{-0.22}$, $0.28^{+0.81}_{-0.16}$ counts/keV in the region from 300 to 400 keV for the spectra (b) and (c), respectively, which means that the background level was reduced to 1/170 and 1/230 compared to the spectrum (a). A Poisson distribution was assumed for evaluation of the statistical errors at the 68% confidence level.

When we assume that the contributions other than E1 transition are negligibly small in the last transition, the probability that Ξ^- reaches the $(n, n - 1)$ state, $P'_{\Xi^-}(n, n - 1)$, is obtained as

$$P'_{\Xi^-}(n, n - 1) = P_{\Xi^-}(n + 1, n) \cdot BR(E1, (n + 1, n) \rightarrow (n, n - 1)) \quad (4)$$

where $P_{\Xi^-}(n + 1, n)$ is the probability that Ξ^- reaches the upper state, which includes Auger processes and the electromagnetic transitions with $\Delta l \geq 2$. Experimentally, $P'_{\Xi^-}(n, n - 1)$ was given as

$$P'_{\Xi^-}(n, n - 1) = \frac{Y_{X\text{-ray}}}{Y_{\sigma\text{-stop}} \cdot R(Z) \cdot \epsilon_{\text{Ge}} \cdot \epsilon_{\text{BGO}}}, \quad (5)$$

where $Y_{X\text{-ray}}$ is the yield of the $(n + 1, n) \rightarrow (n, n - 1)$ transition X-ray, $Y_{\sigma\text{-stop}}$ is the number of σ -stop events, $R(Z)$ is the probability that the Ξ^- is captured by a Z atom, ϵ_{Ge} is the efficiency of the Ge detector system, and ϵ_{BGO} is the signal survival ratio in the BGO suppression. We identified 2208 σ -stop events from all the emulsion modules. However, only the σ -stop events from 90 emulsion modules, which had calibration data to evaluate the efficiency of the Ge array, were used in the following discussion. The number of observed σ -stop events for these 90 emulsion modules was 1889. Considering the misclassification and the π^- contamination (see Sect. 4.2), the number of Ξ^- hyperons included in this event set was estimated to be 1579 ± 53 . Of the stopped Ξ^- hyperons, $(56.8 \pm 4.6)\%$ are absorbed by the heavy (Br and Ag) atoms, and the remainder $(43.2 \pm 3.8)\%$ are absorbed by light (C, N, and O) atoms [19]. The E07 emulsion composition was the same as that of E373 within the margin of error. Among Ξ^- hyperons captured by the heavy atoms, the $R(Z)$ values for each of the Br or Ag atoms were assumed to be proportional to Z . Figure 6 shows the obtained energy spectra with the BGO suppression around the Br($7I \rightarrow 6H$) transition at 316 keV (top left) and the Ag($8J \rightarrow 7I$) transition at 370 keV (top right). The P'_{Ξ^-} values for those transitions were evaluated according to Eq. (5). The upper limit of P'_{Ξ^-} was evaluated based on the method in Ref. [31], taking into account a systematic uncertainty of 13.7%, indicated by the solid line in Fig. 6 (bottom). In most energy regions, the obtained upper limit of the P'_{Ξ^-} values exceeded 1; thus the experimental sensitivity should be improved.

From the obtained background level and estimated X-ray yield, the experimental sensitivity in the statistics of this work is discussed. The background level of the σ -stop event is 0.34 counts/keV. In the case of Ξ^- Ag atoms, assuming that the $P_{\Xi^-}(8J)$ value is 0.6 and $BR(E1, 8J$

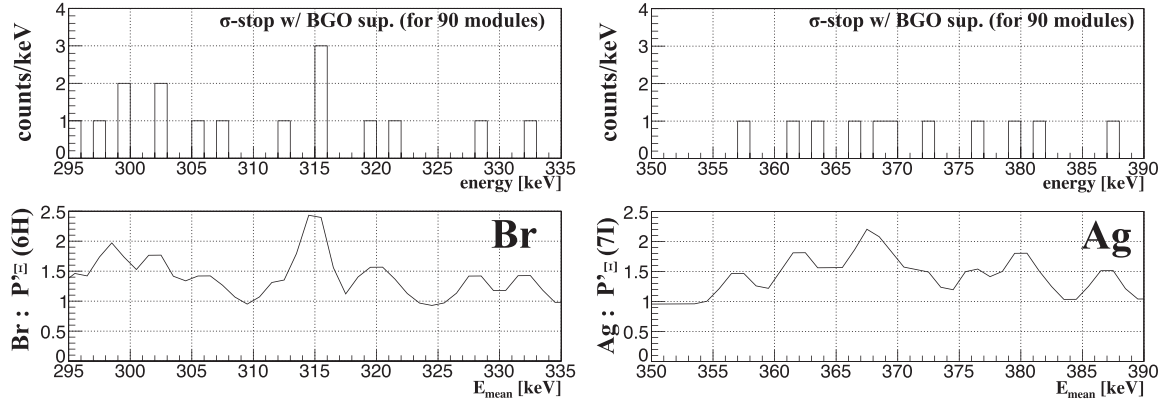


Fig. 6. (Top) X-ray spectra around the Br($7I \rightarrow 6H$) transition at 316 keV (top left) and the Ag($8J \rightarrow 7I$) transition at 370 keV (top right). Only the data for σ -stop events for 90 emulsion modules were filled, and the BGO suppression was applied. (Bottom) The obtained upper limit of the P'_{E-} value for the above two transitions.

$\rightarrow 7I$) is 0.88 (E. Friedman and A. Gal, private communications), the X-ray yield for the Ag($8J \rightarrow 7I$) transition is estimated to be 1.9 counts from Eq. (5). If the level width is negligible with respect to the detector resolution, signal-to-noise ratio, S/\sqrt{N} , the value in the $\pm 3\sigma$ peak region is obtained as 1.5. Thus, the E^- Ag atomic X-ray peak with a 3.4σ significance would be observed with five times the present statistics. Even assuming that the level width is broadened as predicted by the ND model, the X-ray would be observed with a 2.8σ significance.

The stopped E^- selection using emulsion images dramatically reduced the background. However, it was found that the efficiency of the emulsion analysis was low as $\sim 40\%$. The main reason for this inefficiency seems to be that the E^- track cannot be connected between the SSD tracking detector and the emulsion due to the smaller flatness of the emulsion plate at the stacking into the module. It is expected that efficiency will be improved by taking measures to install the emulsion plates without distorting them, and improving analysis methods. There is room to improve the statistics by a factor of 2.5. These improvements, plus a 2 times increase in the data-taking period, will allow X-ray observations.

6. Summary

The first E^- atomic X-ray spectroscopy, referred to as the J-PARC E07 experiment, was conducted using the 1.8 GeV/c K^- beam at J-PARC to investigate the E^- -nucleus interaction by measuring the shift and width of the last transitions. To reject the significant background due to the in-flight E^- decay, a novel method in which the stopped E^- events were identified by a coincidence of magnetic spectrometers, nuclear emulsion, and X-ray detectors was employed. The X-rays associated with the last transitions of E^- Br and E^- Ag atoms, i.e., Br($7I \rightarrow 6H$) and Ag($8J \rightarrow 7I$), were measured by the Ge detector array. The X-ray spectra were obtained by selecting the σ -stop and ρ -stop events by emulsion analysis. In addition, “ ρ -stop with Auger electrons” and/or “ σ -stop without short prong” selections were required for X-rays from heavy E^- atoms. Although no evident peak was observed due to the insufficient experimental sensitivity, the background level was drastically reduced to 1/170 by employing the triple coincidence measurement. With improved emulsion analysis and statistics, the method established in this work will successfully identify E^- atomic X rays in the future.

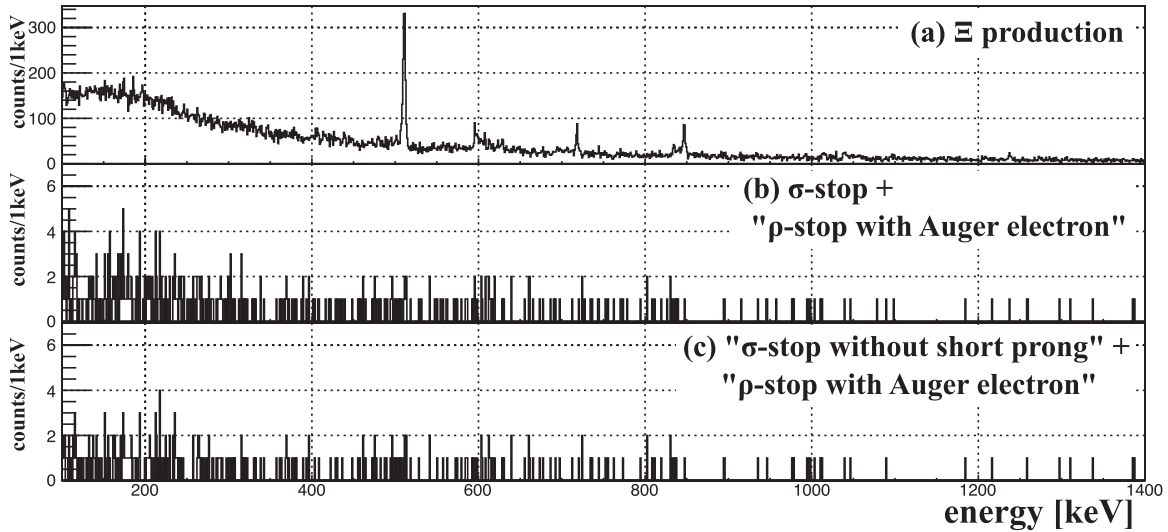


Fig. A1. X-ray spectra for the entire effective energy range of the Ge array (a) for the Ξ^- production by (K^- , K^+) reaction (top), (b) for the σ -stop events and the “ ρ -stop with Auger electron” events (middle), and (c) for the “ σ -stop without short prong” events and “ ρ -stop with Auger electron” events (bottom).

Acknowledgements

We would like to thank the staff of the J-PARC accelerator and the Hadron Experimental Facility for their support during the experiment. We are grateful to the FUJIFILM Corporation for the production of the emulsion gel. The emulsion was stored in Kamioka mine before beam irradiation. We thank the staff of the Kamioka Observatory, ICRR. We also thank the staff of the KEK Computing Research Center for allowing us to use their computational resources. This work was supported by JSPS KAKENHI Grant Numbers JP23224006, JP16H02180, JP16H02190, JP25105512, JP18H05403, JP24105002, and JP17J02360, and MEXT KAKENHI Grant Numbers JP15001001 and JP24105002.

Appendix A. X-ray spectrum in entire effective energy range

Energy spectra in the entire effective energy region of our Ge array were obtained as shown in Fig. A1. The event identification approaches leading to spectra (a), (b), and (c) are explained in the main text. They were obtained from the data of all the scanned emulsion modules with the BGO suppression applied. Spectrum (a) is a photon energy spectrum for all the Ξ^- production events, in which some known γ -ray peaks were identified, such as e^+e^- annihilation (511 keV), ^{74}Ge (596 keV), ^{10}B (718 keV), ^{72}Ge (834 keV), and ^{56}Fe (847 keV). These γ rays were caused by the scattered beam particles and secondary particles/photons from the beam reaction in the target hitting the Ge detectors and the surrounding materials, such as a magnetic shield made of iron. Peak structure was searched for, and the peak significance was obtained as shown in Fig. A2 for spectra (b) and (c).

Appendix B. Branching ratio of the upper transition

Although the last transition was predicted to be $\text{Br}(7I \rightarrow 6H)$ or $\text{Ag}(8J \rightarrow 7I)$ by assuming theoretical models of the Ξ^- -nucleus strong interaction, it is possible that many Ξ^- hyperons are absorbed before the $\text{Br}(7I \rightarrow 6H)$ or $\text{Ag}(8J \rightarrow 7I)$ transitions. Thus, the upper limits of the P_{Ξ^-} values for the upper transitions were also derived. The energy spectra and the P_{Ξ^-} values for the upper transitions, i.e., the $\text{Br}(8J \rightarrow 7I)$ transition at 206 keV and the $\text{Ag}(9K \rightarrow 8J)$ transition at 255 keV, are shown in Fig. B1. For the (b) σ -stop and “ ρ -stop with Auger electron” events,

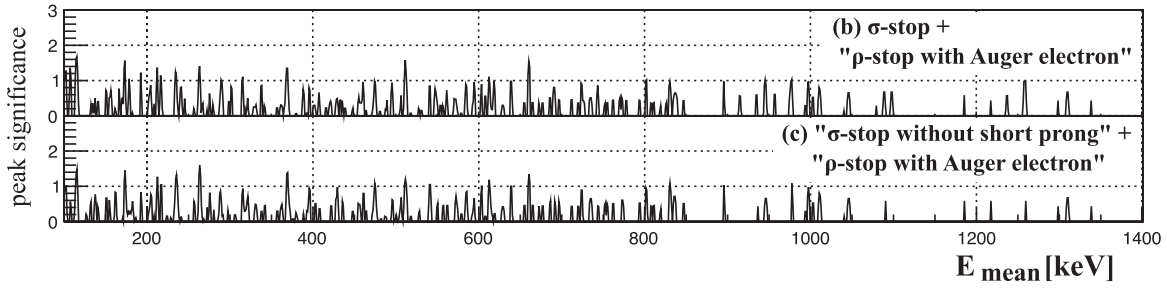


Fig. A2. Peak significance for the (b) and (c) spectra in Fig. A1.

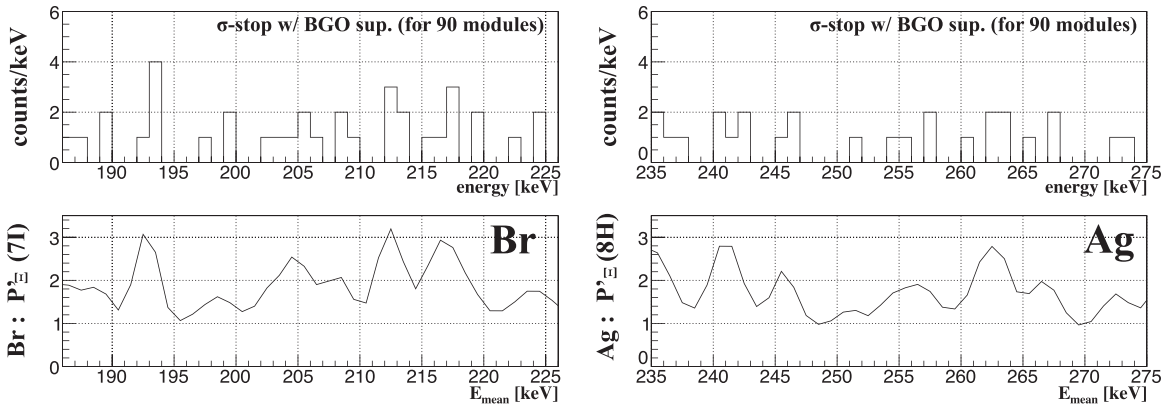


Fig. B1. (Top) X-ray spectra around the Br($8J \rightarrow 7I$) transition at 206 keV (top left) and the Ag($9K \rightarrow 8J$) transition at 255 keV (top right). Only the data for σ -stop events from 90 emulsion modules were used with the BGO suppression applied. (Bottom) The obtained upper limit of the P_{E-} values for the two transitions above.

the background level was obtained as $1.08^{+1.17}_{-0.72}$ counts/keV at 206 keV and $0.78^{+1.06}_{-0.52}$ counts/keV at 255 keV, respectively. The P_{E-} values were evaluated by the procedure described in Sect. 5. For both of the upper transitions, the upper limits of the P_{E-} values exceeded 1. Even though the upper transition has a larger yield and a narrower width, it is more difficult to measure than the last transition due to the higher background level at lower energies.

References

- 1 O. Hashimoto and H. Tamura, Prog. Part. Nucl. Phys. **57**, 564 (2006).
- 2 A. Gal, E. V. Hungerford and D. J. Millener, Rev. Mod. Phys. **88**, 035004 (2016).
- 3 C. J. Batty, E. Friedman and A. Gal, Prog. Theor. Phys. Suppl. **117**, 227 (1994).
- 4 J. Mareš, E. Friedman, A. Gal and B. K. Junnings, Nucl. Phys. A **594**, 311 (1995).
- 5 H. Noumi et al., Phys. Rev. Lett. **89**, 072301 (2002).
- 6 K. Miwa et al. [J-PARC E40 Collaboration], Phys. Rev. C **104**, 045204 (2021).
- 7 K. Miwa et al. [J-PARC E40 Collaboration], Phys. Rev. Lett. **128**, 072501 (2022).
- 8 T. Fukuda et al. [E224 Collaboration], Phys. Rev. C **58**, 1306 (1998).
- 9 P. Khaustov et al. [The AGS E885 Collaboration], Phys. Rev. C **61**, 054603 (2000).
- 10 KEK E176 Collaboration, S. Aoki et al., Nucl. Phys. A **828**, 191 (2009).
- 11 J. K. Ahn et al. [E373 (KEK-PS) Collaboration], Phys. Rev. C **88**, 014003 (2013).
- 12 K. Nakazawa et al., Prog. Theor. Exp. Phys. **2015**, 033D02 (2015).
- 13 T. Nagae et al., Proposal for the next E05 run with the S-2S spectrometer: Proposal for Nuclear and Particle Physics Experiments at J-PARC (2018) (available at: http://j-parc.jp/researcher/Hadron/en/pac_1801/pdf/P70_2018-10.pdf, date last accessed May 21, 2022), J-PARC Center, Ibaraki, Japan.

- 14 K. Imai, K. Nakazawa, and H. Tamura, J-PARC E07 experiment: Systematic study of double-strangeness system with an emulsion-counter hybrid method: Proposal for Nuclear and Particle Physics Experiments at J-PARC (2006) (available at: http://j-parc.jp/researcher/Hadron/en/pac_0606/pdf/p07-Nakazawa.pdf, date last accessed May 21, 2022), J-PARC Center, Ibaraki, Japan.
- 15 H. Ekawa et al., Prog. Theor. Exp. Phys. **2019**, 021D02 (2019).
- 16 S. H. Hayakawa et al., Phys. Rev. Lett. **126**, 062501 (2021).
- 17 M. Yoshimoto et al., Prog. Theor. Exp. Phys. **2021**, 073D02 (2021).
- 18 C. J. Batty, E. Friedman and A. Gal, Phys. Rep. **287**, 385 (1997).
- 19 A. M. M. Theint, H. Ekawa, A. Kasagi, S. Kinbara, M. Sweet, K. T. Tint, C. S. Yoon, J. Yoshida, M. Yoshimoto and K. Nakazawa, Prog. Theor. Exp. Phys. **2019**, 021D01 (2019).
- 20 C. J. Batty, E. Friedman and A. Gal, Phys. Rev. C **59**, 295 (1999).
- 21 Y. Yamamoto, T. Motoba, H. Himeno, K. Ikeda and S. Nagata, Prog. Theor. Phys. Suppl. **117**, 361 (1994).
- 22 M. M. Nagels, T. A. Rijken and J. J. de Swart, Phys. Rev. D **15**, 2547 (1977).
- 23 E. Friedman and S. Okada, Nucl. Phys. A **915**, 170 (2013).
- 24 A. T. M. Aerts and C. B. Dover, Phys. Rev. D **28**, 450 (1983).
- 25 T. Takahashi et al., Nucl. Phys. A **835**, 88 (2010).
- 26 M. Fujita, K. Hosomi, Y. Ishikawa, H. Kanauchi, T. Koike, Y. Ogura, H. Tamura, K. Tanida, M. Uka and T. O. Yamamoto, Nucl. Instrum. Meth. A **1042**, 167439 (2022).
- 27 J. Myrheim and L. Bugge, Nucl. Instrum. Meth. A **160**, 43 (1979).
- 28 H. Ekawa, Observation of a Double- Λ Hypernucleus $\Lambda\Lambda\text{Be}$ with Hybrid Emulsion Method at J-PARC, Doctoral Thesis, Kyoto University (2019).
- 29 S. H. Hayakawa, Study of Ξ -nucleus interaction by measurement of twin hypernuclei with hybrid emulsion method, Doctoral Thesis, Osaka University (2019).
- 30 M. K. Soe, R. Goto, A. Mishina, Y. Nakanishi, D. Nakashima, J. Yoshida and K. Nakazawa, Nucl. Instrum. Meth. A **848**, 66 (2017).
- 31 G. J. Feldman and R. D. Cousins, Phys. Rev. D **57**, 3873 (1998).